Institut de Physique du Globe de Paris

Ecole doctorale des Sciences de la Terre

Thèse de Doctorat

pour l'obtention du titre de

Docteur en Science

de l'Institut de Physique du Globe de Paris

Specialité : Geophysique

Soutenue par

Clément Thorey

Magmatisme intrusif sur les planétes telluriques

Équipe Planétologie et Sciences Spatiales,

défendue le 5 Décembre, 2013.

Jury :

Directeur:	Chloé Michaut	-	IPGP (Paris)
Co-directeur:	Mark Wieczorek	-	IPGP (Paris)
Rapporteur :		-	
Rapporteur :		-	
Examinateur :		-	
Examinateur :		-	

Remerciements

Je remercie marion rouault mae sans qui tout ceci n'aurait jamais vu le jour ;)

Contents

Résumé de la problématique et résultats principaux

Part I

High-level magmatic systems

Chapter 1

Shallow intrusive magmatism

Contents

1.1 Eruption versus intrusion: review of the magma transport processes within the crust

The transport of magma from deep regions in the Earth to shallower layer occurs through several mechanisms. Hereafter, we review the important processes that control how melts are extracted from their source regions, transported through the crust and intruded into the crust based on the general review made by (*Petford et al.*, 2000).

1.1.1 Partial melting and melt ascent

In the upper mantle, melt and magma (melt plus suspended solids) formed by partial melting of the solid rocks. The melt, which is less dense than the surrounding material, first percolates through the matrix of unmolten

material by buoyancy (*McKenzie*, 1984, 1985). However, percolation acts over small length scale (centimeter to decimeters) and long range ascent mechanism (kilometer-scale) must exist to transport the melt from the source region to the shallow layer of a planet.

Low inertia diapiric ascent has been invoked traditionally as a common ascent mechanism for the melt (*Miller and Paterson*, 1999). However, geological observations show that the melt are rapidly transported within the crust via thin conduit called dykes. Indeed, it is now well accepted that large magma reservoirs formed by repeated

Although low inertia diapiric ascent is still invoked in the ductile lower crust, it is now generally accepted that magmas are rapidly transported within conduit or dyke through the layer of the crust. Indeed, while the ascent velocity of a buoyant diapir is controlled mainly by the viscosity of the host rocks, the average velocity of the dyke is controlled by the viscosity of the melt itself resulting in a much faster ascent.

This melting is less dense and rises by buoyancy, through compaction and percolation, across the matrix of unmolten materials (*McKenzie*, 1984, 1985). Within the curst

Several and it is now well accepted that magma collect into conduit or dyke. Indeed, it is now well accepted that the formation of plutons and magmatic reservoir are the result of sills and dyke and not due to diapirism . How, lack of direct observation made this process still unconstrains.

1.1.2 Emplacement

1.2 Shallow magmatic intrusions on the Earth

1.2.1 Magma budget

1.2.2 Laccolith from Corry et al

1.2.3 Laccolith at Elba island

1.3 Shallow magmatic intrusion on the Moon

1.3.1 Intrusive magmatism on the Moon

1.3.2 Low-slopes domes

1.3.3 Floor-fractured craters

Chapter 2

Previous model for shallow magmatic intrusion

Contents

2.1 Original theoretical framework

2.2 Elastic plated gravity current

At shallow depth in the upper crust, roof lifting is the dominant process by which magma makes room for itself (*Johnson and Pollard*, 1973; *Pollard and Johnson*, 1973), which leads to the deformation and bending of the overlying strata. Such system is commonly modeled as an isoviscous elastic-plated gravity current, i.e. an isoviscous fluid spreading beneath a thin elastic sheet of thickness d_c and above a rigid layer (*Michaut*, 2011; *Bunger and Cruden*, 2011) (Figure 2.1). The behavior of isoviscous elastic-plated gravity current have been largely discussed in the past few years in both carthesian (*Michaut*, 2011; *Bunger and Cruden*, 2011; *Hewitt et al.*, 2014) and axisymmetrical geometry

(*Michaut et al.*, 2013; *Lister et al.*, 2013). This section details a summary of the results for an isoviscous fluid of density ρ_m and viscosity η, supplied at a continuous rate $Q(t)$ through a cylindrical conduit of diameter a at the center, in an axisymmetrical geometry (Figure 2.1). This model will constitute the reference for more elaborate models in the manuscript.

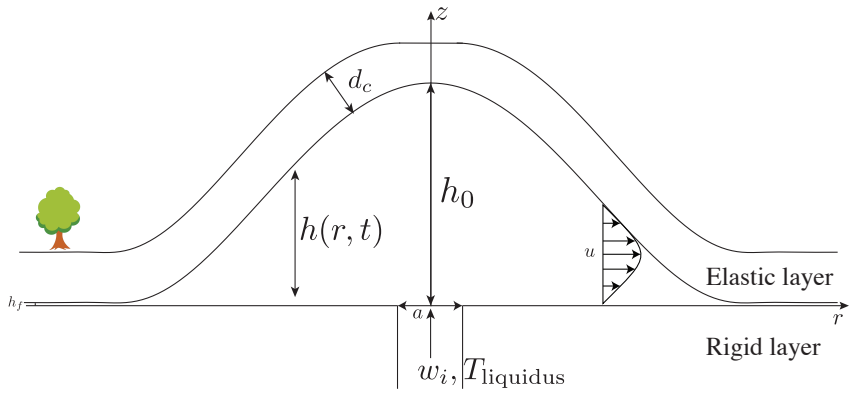

Figure 2.1: Model geometry and parameters.

2.2.1 Governing equation

Driving pressure

The intrusion develops over a length scale Λ that is much larger than its thickness H ($\varepsilon = H/\Lambda << 1$). In the laminar regime and in axisymmetrical coordinates (r,z), the Navier-stokes equations within the lubrication assumption are

$$-\frac{\partial P}{\partial r} + \frac{\partial}{\partial z}\left(\eta \frac{\partial u}{\partial z}\right) = 0 \tag{2.1}$$

$$-\frac{\partial P}{\partial z} - \rho_m g = 0 \tag{2.2}$$

where $u(r,z,t)$ is the radial velocity, g is the standard acceleration due to gravity and $P(r,z,t)$ is the pressure within the fluid. Integration of (2.2) thus gives the total pressure $P(r,z,t)$ within the flow. When the vertical deflection deflection $h(r,t)$ of the upper elastic layer is small compared to its thickness d_c, i.e $h << d_c$, we can neglect stretching of the upper layer and only consider bending stresses. Therefore, the total pressure $P(r,z,t)$ at a level z in the intrusion is the sum of four contributions: the weight of the magma and of

the upper layer, the bending pressure P_b and the atmospheric pressure P_0

$$P = \rho_m g(h - z) + \rho_r g d_c + P_b + P_0 \tag{2.3}$$

where $h(r,t)$ is the intrusion thickness and ρ_r the density of the surrounding rocks. The bending pressure is given by the force per unit area that is necessary for a vertical displacement h of the thin elastic plate (*Turcotte and Schubert*, 1982)

$$P_d = D\nabla^4 h \tag{2.4}$$

where D is the flexural rigidity of the thin elastic layer, that depends on the Young's modulus E, Poisson's ratio ν^* and on the elastic layer thickness d_c as $D = Ed_c^3/\left(12(1-\nu^*)\right)$.

Velocity field

At the contact with the elastic sheet $z = h(r,t)$, the no-slip boundary condition is present and so, the tangential velocity is zero and the normal velocity is the change in height $(\partial h/\partial t)$. With $\vec{n}$ the normal to the surface and $\vec{t}$ the tangent, we have

$$\vec{n} \cdot (u, w) = \frac{\partial h}{\partial t} \tag{2.5}$$

$$\vec{t} \cdot (u, w) = 0. \tag{2.6}$$

The tangent vector is $\vec{t} = (1, \partial h/\partial r)$. However, within the lubrication assumption, the vertical component of the tangent vector scales as ε and thus, is negligible compared to the radial component. Therefore, the boundary condition (2.6) reduces to $u(r, z = h, t) = 0$. At the base of the flow, the same boundary condition hold and $u(r, z = 0, t) = 0$.

Equation (2.1) is integrated twice as a function of z using these boundary conditions and the horizontal velocity is

$$u(r,z,t) = \frac{1}{2\eta}\frac{\partial P}{\partial r}\left(z^2 - hz\right) \tag{2.7}$$

Injection rate

The effective overpressure ΔP^* driving the flow in the feeder conduit decreases as the intrusion thickens and is given by

$$\Delta P^* = \Delta P - \rho_m g h_0 \tag{2.8}$$

where $h_0(t)$ is the maximum intrusion thickness at the center $r = 0$ and ΔP is the initial driving pressure or the overpressure at the base of the dyke ($z = -Z_c$).

In (2.8), the bending pressure at then center, which scale as $\mathrm{D}h_0(t)/R(t)^4$ where $R(t)$ is the blister radius, has been neglected. Although it tends to infinity at the initiation of the flow, it rapidly vanishes as the blister spreads and the hydrostatic pressure $\rho_m g h_0$ becomes the main contribution to the pressure at the center. In addition, the model assumes a large aspect ratio for the blister and does not consider the initiation of the flow.

Finally, assuming a Poiseuille flow within the cylindrical feeding conduit, the vertical injection velocity $w_i(r,t)$ and injection rate $Q(t)$ are given by

$$w_i = \begin{cases} \frac{\Delta P^*}{4\mu Z_c}(\frac{a^2}{4} - r^2) & r \leq \frac{a}{2} \\ 0 & r > \frac{a}{2} \end{cases} \tag{2.9}$$

$$Q = Q_0(1 - \frac{\rho_m g h_0}{\Delta P}) \tag{2.10}$$

where $Q_0 = (\pi \Delta P^* a^4) \,/\, (128 \eta Z_c)$.

Mass conservation

The fluid is assumed incompressible and a global statement of mass conservation gives

$$\frac{\partial h}{\partial t} + \frac{1}{r}\frac{\partial}{\partial r}\left(r \int_0^h u dz\right) = w_i \tag{2.11}$$

and using (2.7), we find that the equation for the evolution of the thickness in time and space reads

$$\frac{\partial h}{\partial t} = \frac{\rho_m g}{12\eta r}\frac{\partial}{\partial r}\left(r h^3 \frac{\partial h}{\partial r}\right) + \frac{D}{12\eta r}\left(r h^3 \frac{\partial}{\partial r}\nabla^4 h\right) + w_i. \tag{2.12}$$

It is composed of three different terms on the right hand side. The first term represents gravitational spreading, i.e. spreading of the blister under its own weight. The second term represents the squeezing of the flow by the upper elastic layer. Both term are negative and induces spreading. The last term represents fluid injection and is positive.

2.2.2 Dimensionless equations

Equations (3.97) and (2.12) are nondimensionalized using a horizontal scale Λ, a vertical scale H and a time scale τ given by

$$\Lambda = \left(\frac{D}{\rho_m g}\right)^{1/4} \tag{2.13}$$

$$H = \left(\frac{12\eta Q_0}{\rho_m g \pi}\right)^{\frac{1}{4}} \tag{2.14}$$

$$\tau = \frac{\pi \Lambda^2 H}{Q_0} \tag{2.15}$$

where scales are chosen such that $Q_0 = \pi\Lambda^2 H/\tau$. The length scale represents the flexural wavelength of the upper elastic layer, i.e. the length scale at which bending stresses and gravity contributes equally to flow. The height scale H is the thickness of a typical gravity current and the time scale τ is the characteristic time to fill up a cylindrical flow of radius Λ and thickness H at constant rate Q_0. In addition, we can define a horizontal velocity scale $U = \Lambda/\tau = (\rho_m g H^3) / (12\eta_h \Lambda)$.

The dimensionless equation is

$$\begin{aligned} \frac{\partial h}{\partial t} &= \frac{1}{r}\frac{\partial}{\partial r}\left(r h^3 \frac{\partial h}{\partial r}\right) + \frac{1}{r}\left(r h^3 \frac{\partial}{\partial r}\nabla^4 h\right) \\ &+ \frac{32}{\gamma^2}\left(\frac{1}{4} - \frac{r^2}{\gamma^2}\right)\left(1 - \frac{h_0}{\sigma}\right) \end{aligned} \tag{2.16}$$

where the last term is replaced by zero for $r > \gamma/2$. γ and σ are two dimensionless numbers that control the dynamics of the flow

$$\gamma = \frac{a}{\Lambda} \tag{2.17}$$

$$\sigma = \frac{\Delta P}{\rho_m g h}. \tag{2.18}$$

γ is the dimensionless radius of the conduit, it does not significantly influence the flow and is set to 0.02 in the following (*Michaut and Bercovici*, 2009; *Michaut*, 2011). σ is the normalized pressure head, i.e., the ratio between the initial overpressure driving the flow and the weight of the magma at the center.

2.2.3 Need for regularization

One of the main mathematical difficulty in solving equation (2.16) arises at the contact line. Indeed, the assumption that the thickness of the fluid tends

to zero at the contact line leads to divergent viscous stresses, and hence, the theoretical immobility of the blister (*Flitton and King*, 2004; *Lister et al.*, 2013; *Hewitt et al.*, 2014). This problem, known a the contact-line paradox, is a well know problem for surface-tension driven flow such as the spreading of a water droplet (*Bertozzi*, 1998; *Snoeijer and Andreotti*, 2013).

The formal proof have been derived by *Flitton and King* (2004) and can be derived as follow. Suppose that (2.16) has a solution and the solution has the form $h \sim A(t)(R(t)-r)^\alpha$ near the contact line. As $r \to R(r)$, the bending term dominates the gravitational term and (2.16) reduces to

$$\frac{\partial h}{\partial t} = \frac{1}{r}\frac{\partial}{\partial r}\left(rh^3\frac{\partial}{\partial r}\nabla^4 h\right). \tag{2.19}$$

Injecting the solution into (2.19) and keeping only the leading powers of $R-r$ gives

$$\frac{\partial R}{\partial t}A\alpha\,(R-r)^{\alpha-1} + \frac{\partial A}{\partial t}\,(R-r)^\alpha = A^4\alpha(\alpha-1)(\alpha-2)(\alpha-3)(\alpha-4)(\alpha-5)(R-r)^{4\alpha-6}$$

The second term on the left is small compared to the first as the blister grows mainly by spreading at the tip and therefore, by equating the exponent of $R-r$, we obtain $\alpha = 5/3$, and by equating the coefficients, we deduce

$$\frac{\partial R}{\partial r} = -\frac{280}{243}A^3. \tag{2.20}$$

It shows that (2.16) can only have retreating contact line ($dR/dt < 0$) but not with advancing contact line ($dR/dt > 0$) (*Lister et al.*, 2013; *Flitton and King*, 2004).

To mitigate this problem, one common approach is to add a thin pre-wetting film, with thickness h_f such that $h \to h_f$ as $r \to \infty$. While the solution will depend upon the pre-wetted film thickness h_f and will not show any convergence properties when $h_f \to 0$, we will see that the dependence in h_f is weak and the difference between different values for h_f will be relatively small (*Lister et al.*, 2013; *Hewitt et al.*, 2014). Unless otherwise specified, we will consider $h_f = 5 \cdot 10^{-3}$ in the manuscript.

2.3 Regime of propagations

For a small pre-wetting film thickness, i.e. $h_f/H << 1$, the numerical resolution of the equation (3.26) shows three spreading regimes: a bending regime where gravity is negligible, a viscous gravity current regime where bending is negligible and a regime of lateral propagation (*Michaut*, 2011; *Bunger and Cruden*, 2011; *Lister et al.*, 2013).

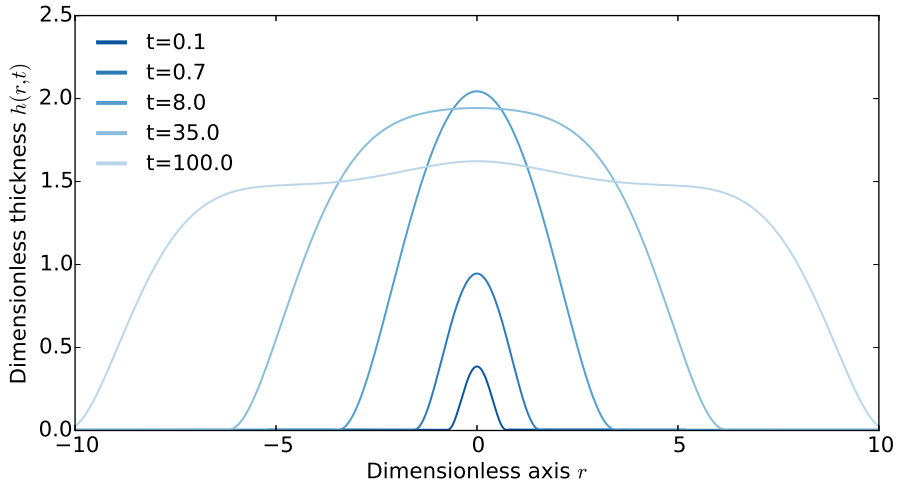

Figure 2.2: Shape of the flow, i.e. thickness $h(r,t)$ as a function of the radial axis r at five different times indicated on the plot. Variables are dimensionless and one needs to multiply by the characteristic scales (thickness, length or time given by (2.14), (2.13) or (2.15)) to obtain dimensional values. For $t < 10$, the intrusion is in the bending regime whereas for $t > 10$ the intrusion is in the gravity current regime.

2.3.1 Bending regime

At early times, when $R << \Lambda$, gravity is negligible and the dynamics of the spreading is governed by the bending of the upper layer. In addition, if $h_0 << \sigma$, the overpressure ΔP driving the flow is much larger than the weight of the blister at the center and the injection rate can be considered constant.

In that case, the spreading is very slow and the interior has uniform pressure $P = \nabla^4 h$. The flow is bell-shaped and its thickness is given by

$$h(r,t) = h_0(t)\left(1 - \frac{r^2}{R^2(t)}\right)^2 \tag{2.21}$$

with $h_0(t)$ the thickness of the intrusion at the center (*Michaut*, 2011; *Lister et al.*, 2013). In this regime, *Lister et al.* (2013) have shown that the spreading is controlled by the propagation of a peeling by bending wave at the intrusion front with dimensionless velocity c

$$c = \frac{\partial R}{\partial t} = h_f^{1/2}\left(\frac{\kappa}{1.35}\right)^{5/2} \tag{2.22}$$

where $\kappa = \partial^2 h/\partial r^2$ is the dimensionless curvature of the interior solution. Using the propagation law (2.22) and the form of the interior solution (2.21),

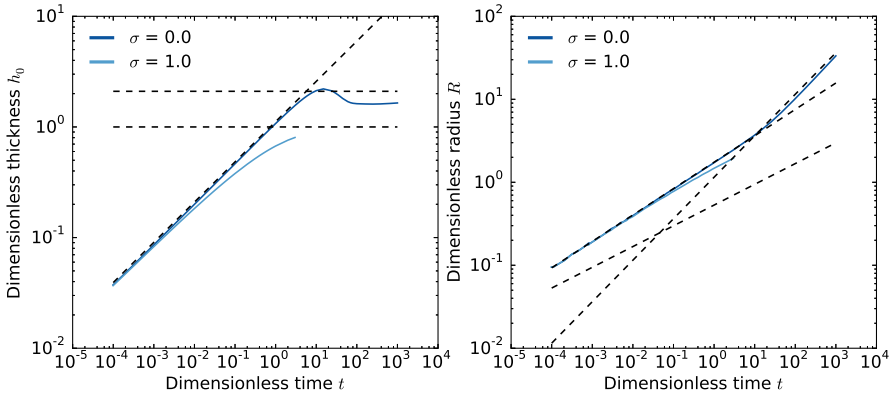

Figure 2.3: Left: Dimensionless thickness at the center h_0 versus dimensionless time t for different dimensionless number σ indicated on the plot. Dashed-lines represent the scaling laws in the different regimes. Right: Dimensionless radius R versus dimensionless time t for the same dimensionless number σ. Dashed-lines represent the scaling laws in the different regimes.

they find that the radius and the height of the intrusion are given by similarity solutions

$$R(t) = 2.2 h_f^{1/22} t^{7/22} \tag{2.23}$$

$$h_0(t) = 0.67 h_f^{-1/11} t^{8/22}. \tag{2.24}$$

where the numerical pre-factor have been matched to our simulations.

2.3.2 Gravity current regime

In contrast, when the radius R becomes much larger than Λ ($R >> \Lambda$), the weight of the intrusion becomes dominant over the bending terms. The pressure is given by the hydrostatic pressure $P = h$ and the intrusion enters a classical viscous gravity current regime where bending terms only affect the solution near the intrusion edge (*Huppert*, 1982; *Michaut*, 2011; *Lister et al.*, 2013). In this second regime, the radius evolves as $t^{1/2}$ and the thickness tends to a constant

$$R(t) = 0.715 t^{1/2} \tag{2.25}$$

$$h_0 = 1.86 \tag{2.26}$$

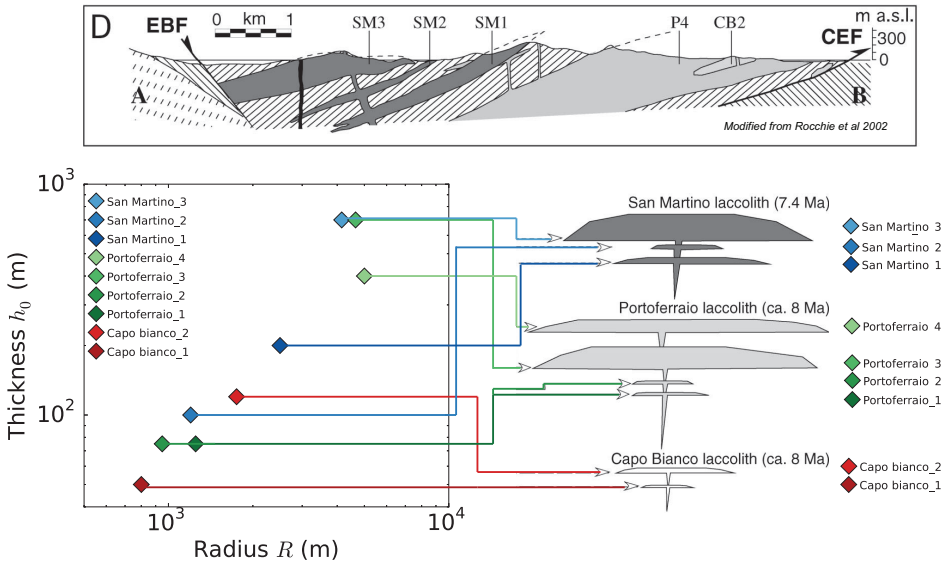

Figure 2.4:

2.3.3 Lateral propagation

Once $h_0 \to \sigma$, the flow is thick enough to compensate for the initial overpressure. The thickness at the center remains constant and the flow enters a regime of lateral propagation, where only its radius $R(t)$ is to increase (*Michaut*, 2011). In this regime, except at the center when it redistributes the pressure over a length scale Λ, the bending term is negligible compared to the gravitational term. *Michaut* (2011) has shown that in this regime, the thickness is constant and the radius evolves as $t^{1/4}$

$$R(t) = \left(\frac{\sigma^3 t}{4\pi}\right)^{1/4} \tag{2.27}$$

$$h_0 = \sigma \tag{2.28}$$

2.4 Application to the Earth, Moon and Mars

2.5 Discussion

Table 2.1: Range of values for the model parameters

Parameters	Symbol	Range of values	Unit
Depth of intrusion	d_c	$0.1 - 5$	km
Young's Modulus	E	$10 - 100$	GPa
Poisson's ratio	ν^*	0.25	
Gravity	g	9.81	m s^{-2}
Magma density	ρ_m	$2800 - 3200$	kg m^{-3}
Magma viscosity	η	$1 - 10^4$	Pa s
Feeder dyke width	a	$1 - 100$	m
Depth of the melt source	Z_c	$5 - 500$	km
Initial overpressure	ΔP	$5 - 50$	MPa
Injection rate	Q_0	$10p{-}3 - 0.1$	m^3 s^{-1}
Crust density	ρ_r	2500	kg m^{-3}
Characteristic scales	**Symbol**	**Range of values**	**Unit**
Height scale	H	$0.1 - 10$	m
Length scale	Λ	$1 - 12$	km
Time scale	τ	$10^{-1} - 10$	years

Table 2.2: Dimensionless numbers

		Complex craters	Simple craters
Symbol	Description	Range of values	Range of values
γ	Normalized source width	$10^{-4} - 10^{-2}$	$10^{-4} - 10^{-2}$
ζ	Normalized wall zone width	$0.05 - 0.13$	0.25
Ψ	Thickening term	$0.3 - 8$	$0.2 - 4$
Ξ	Hydrostatic term	$20 - 400$	$20 - 200$
Θ	Elastic term	$10^{-7} - 0.1$	$10^{-3} - 10$
Ω	Density ratio	1.2	1.2
Φ	Upper layer aspect ratio	4500	1200
σ	Normalized pressure head	$0.6 - 100$	$0.6 - 100$

Part II

Theoretical model for the cooling of elastic-plated gravity current and applications to laccolith on the Earth and Moon

Chapter 3

Model for a cooling elastic-plated gravity current

Contents

We present here a general model, based on the elastic-plated gravity current model developed in the last section, to account for the cooling of the magmatic intrusion.

3.1 Theory

3.1.1 Formulation

We model an axisymmetric fluid blister of thickness $h(r,t)$ below an elastic layer of constant thickness d_c and above a semi infinite rigid layer (*Michaut*, 2011) (Figure 3.1) The fluid is injected continuously at the base and center of the blister at a rate $Q(t)$ through a conduit of diameter a. The hot fluid is intruded at temperature T_i and cools through the top and the bottom by conduction in the surrounding medium, whose temperature T_s is allowed to increase with time.

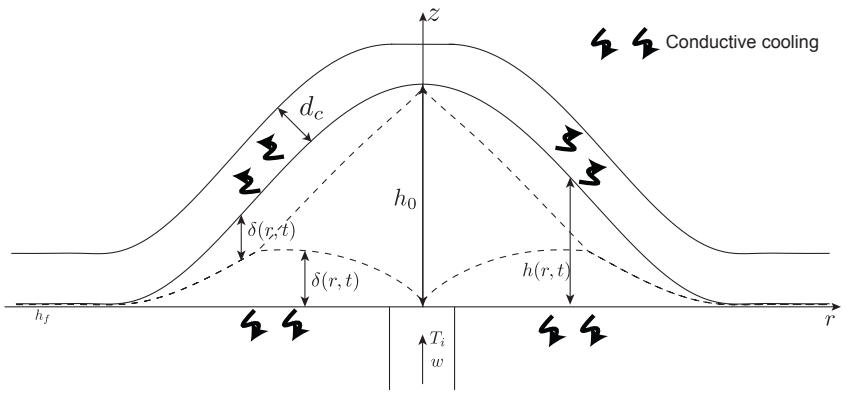

Figure 3.1: Model geometry and parameters.

As it cools, the viscosity of the fluid increases following a prescribed rheology $\eta(T)$ bounded between two values: the viscosity of the hottest fluid η_h at temperature T_i and the viscosity of the coldest fluid η_c at temperature T_0.

3.1.2 Equation for the thickness

For a cooling elastic-plated gravity current, the velocity fields depends on the viscosity, which itself depends on the temperature. Without knowledge on the form of the rheology $\eta(T)$, integrating twice (2.1) using no-slip boundary conditions at the top and the bottom now gives

$$u(r,z,t) = \frac{\partial P}{\partial r}\left(I(z) - I(h)\frac{z}{h}\right) \tag{3.1}$$

with

$$I(z) = \int_0^z \frac{z^*}{\eta(T)} dz^* \tag{3.2}$$

where the driving pressure $P(r,z,t)$ is given by (2.3). However, instead of plugging in this expression in (2.11) as in section 2.2.1, we develop another approach which takes into account the symmetry of the velocity around $h/2$. Indeed, as we will see in the next section, this property comes out naturally from the symmetry of the used vertical temperature structure which implies the same symmetry for the viscosity $\eta(T)$.

Integrating once (2.1) as a function of z using the symmetry around $h/2$ gives

$$\frac{\partial u}{\partial z} = \frac{1}{\eta}\frac{\partial P}{\partial r}\left(z - \frac{h}{2}\right) \tag{3.3}$$

and therefore, the velocity $u(r,z,t)$ reads

$$u(r,z,t) = \frac{\partial P}{\partial r} I_0(z) \tag{3.4}$$

with

$$I_0(z) = \int_0^z \frac{1}{\eta(T)} \left(y - \frac{h}{2} \right) dy \tag{3.5}$$

Moreover, we have that

$$\int_0^h u dz = -\int_0^h \frac{\partial u}{\partial z} z dz \tag{3.6}$$

and therefore, the statement of mass conservation (2.11) can be written

$$\frac{\partial h}{\partial t} = \frac{1}{r} \frac{\partial}{\partial r} \left(r \int_0^h \frac{\partial u}{\partial z} z dz \right) + w_i \tag{3.7}$$

where we can now plug in (3.3) to finally obtain

$$\frac{\partial h}{\partial t} = \frac{1}{r} \frac{\partial}{\partial r} \left(r \left(\rho_m g \frac{\partial h}{\partial r} + D \frac{\partial}{\partial r} \left(\nabla^4 h \right) \right) I_1(h) \right) + w_i. \tag{3.8}$$

with

$$I_1(z) = \int_0^z \frac{1}{\eta(T)} \left(y - \frac{h}{2} \right) y dy \tag{3.9}$$

3.1.3 Heat transport equation

3.1.3.1 Local energy conservation

In the laminar regime and in axisymmetrical coordinates (r,z), the local energy conservation equation within the lubrication assumption is written as

$$\frac{D}{Dt} \left(\rho_m C_{p,m} T + \rho_m L (1 - \phi) \right) = k_m \frac{\partial^2 T}{\partial z^2} \tag{3.10}$$

where $T(r,z,t)$ is the fluid temperature, $\phi(r,z,t)$ is the crystal fraction in the melt and ρ_m, k_m, $C_{p,m}$ and L are the density, thermal conductivity, specific heat and latent heat of the fluid. In this model, the crystals are considered only as a source/sink of energy as they melt/form during the flow emplacement. In particular, they share the same properties that the fluid itself.

Following a common approximation, we assume that the crystal fraction is a linear function of temperature over the melting interval

$$\phi = \frac{T_L - T}{T_L - T_s} \tag{3.11}$$

where T_S and T_L are the solidus and liquidus temperatures of the magma (*Hort*, 1997; *Michaut and Jaupart*, 2006). With this approximation, the local energy equation (3.10) resumes to

$$\frac{\partial T}{\partial t} + u\frac{\partial T}{\partial r} + w\frac{\partial T}{\partial z} = \frac{\kappa_m}{1 + St^{-1}}\frac{\partial^2 T}{\partial z^2} \tag{3.12}$$

where $u(r, z, t)$ and $w(r, z, t)$ are the radial and vertical fluid velocities, $St = (C_{p,m}(T_L - T_S))/L$ is the Stephan number and κ_m is the fluid thermal diffusivity $\kappa_m = k_m/\rho_m C_{p,m}$. Following *Balmforth and Craster* (2000), we use an integral balance method to solve the heat transport equation (3.12). This theory is based on the integral-balance method of heat-transfer theory of *Goodman* (1958), in which the vertical structure of the temperature field is represented by a known function of depth that approximates the expected solution.

3.1.3.2 Integral balance solution for the temperature $T(r, z, t)$

We model the cooling of the fluid blister through the growth of two thermal boundary layers: one growing downward from the top and a second growing upward from the base. As we consider homogeneous thermal properties for the surrounding rocks, we assume that the two thermal boundary layers grow symmetrically and have the same thickness $\delta(r, t)$. In agreement, the integral-balance approximation we use for the vertical temperature profile $T(r, z, t)$ is

$$T = \begin{cases} T_b - (T_b - T_s)(1 - \frac{z}{\delta})^2 & 0 \leq z \leq \delta \\ T_b & \delta \leq z \leq h - \delta \\ T_b - (T_b - T_s)(1 - \frac{h-z}{\delta})^2 & h - \delta \leq z \leq h \end{cases} \tag{3.13}$$

where $T_b(r, t)$ is the temperature at the center of the flow and $T_s(r, t)$ the temperature at the contact with the surrounding rocks (Figure **??**). The integral balance solution in (3.13) assumes a symmetry around $z = h/2$ and a decrease of the temperature in the two thermal boundary layers down to the surrounding rock temperature T_s (*Balmforth and Craster*, 2000). In addition, it assumes a uniform temperature T_b in between the thermal boundary layers. Then, as the fluid is injected at a temperature T_i, we have $T_b(r, t) = T_i$ when $\delta < h/2$. However, if the two thermal boundary layers connect, then $\delta = h/2$ and T_b decreases such that $T_b \leq T_i$.

3.1.3.3 Integral balance equation

We begin by integrating the local energy conservation (3.12) over the two thermal boundary layers. The integration over the bottom thermal layer, i.e.

from the base, $z = 0$ to a level $z = \delta$ gives

$$\begin{aligned} & \frac{\partial}{\partial t}\left(\delta(\bar{T} - T_b)\right) + \frac{1}{r}\frac{\partial}{\partial r}\left(r\delta(\overline{uT} - \bar{u}T_b)\right) + \delta\left(\frac{\partial T_b}{\partial t} + \overline{u}\frac{\partial T_b}{\partial r}\right) \\ = & -\frac{\kappa_m}{1 + St^{-1}}\left.\frac{\partial T}{\partial z}\right|_{z=0} + w_i(T_i - T_b) \end{aligned} \tag{3.14}$$

where the bar indicate the vertical average over the bottom thermal boundary layer

$$\overline{f} = \frac{1}{\delta}\int_0^\delta f dz,$$

$T_b(r,t)$ is the temperature at $z = \delta$, $w_i(r)$ is the vertical injection velocity and we have used the nullity of the thermal gradient at $z = \delta$ and the local mass conservation

$$\frac{1}{r}\frac{\partial ru}{\partial r} + \frac{\partial w}{\partial z} = 0. \tag{3.15}$$

The integration over the top thermal layer, i.e., from the level, $z = h - \delta$ to the top $z = h$ gives:

$$\begin{aligned} & \frac{\partial}{\partial t}\left(\delta(\bar{T} - T_b)\right) + \frac{1}{r}\frac{\partial}{\partial r}\left(r\delta(\overline{uT} - \bar{u}T_b)\right) + \delta\left(\frac{\partial T_b}{\partial t} + \overline{u}\frac{\partial T_b}{\partial r}\right) \\ = & \frac{\kappa_m}{1 + St^{-1}}\left.\frac{\partial T}{\partial z}\right|_{z=h}. \end{aligned} \tag{3.16}$$

where, in addition to the local mass conservation (3.15) and the fact the thermal gradient at $z = h - \delta$ is equal to zero, we have used the kinematic boundary condition in $z = h(r,t)$

$$\frac{\partial h}{\partial t} + u\frac{\partial h}{\partial r} = w \tag{3.17}$$

The heat balance equation can then be written by adding (3.14) and (3.16) and introducing (3.13)

$$\begin{aligned} & \frac{\partial}{\partial t}\left(\delta(\bar{T} - T_b)\right) + \frac{1}{r}\frac{\partial}{\partial r}\left(r\delta(\overline{uT} - \bar{u}T_b)\right) + \delta\left(\frac{\partial T_b}{\partial t} + \overline{u}\frac{\partial T_b}{\partial r}\right) \\ = & \frac{\kappa_m}{2(1 + St^{-1})}\left(\left.\frac{\partial T}{\partial z}\right|_{z=h} - \left.\frac{\partial T}{\partial z}\right|_{z=0}\right) + \frac{w_i}{2}(T_i - T_b) \end{aligned} \tag{3.18}$$

3.1.3.4 Thermal boundary conditions

At the contact with the surrounding rock, the heat is lost by conduction:

$$k_m\left.\frac{\partial T}{\partial z}\right|_{z=0} = k_r\left.\frac{\partial T_r}{\partial z}\right|_{z=0} \tag{3.19}$$

$$k_m \left.\frac{\partial T}{\partial z}\right|_{z=h} = k_r \left.\frac{\partial T_r}{\partial z}\right|_{z=h} \tag{3.20}$$

where $T_r(r,z)$ is the temperature in the surrounding medium. Assuming a semi infinite layer for the rigid layer below the intrusion, *Carslaw and Jaeger* (1959) show that the temperature T_r in the surrounding rocks can be approximated to a first order by

$$T_r(r,z,t) - T_0 = (T_s - T_0)\,\mathrm{erfc}\left(\frac{-z}{2\sqrt{\kappa_r t}}\right). \tag{3.21}$$

The thickness of the upper layer is equal to the intrusion depth d_c. However, we assume that the depth d_c is large compared to the characteristic length scale for conduction L_c and we use the same approximation to derive T_r above the intrusion

$$T_r(r,z,t) - T_0 = (T_s - T_0)\,\mathrm{erfc}\left(\frac{z-h}{2\sqrt{\kappa_r t}}\right). \tag{3.22}$$

Therefore, the two thermal boundary conditions (3.19) and (3.20) become:

$$k_m \left.\frac{\partial T}{\partial z}\right|_{z=0} = k_r \frac{T_s - T_0}{\sqrt{\pi \kappa_r t}} \tag{3.23}$$

$$k_m \left.\frac{\partial T}{\partial z}\right|_{z=h} = -k_r \frac{T_s - T_0}{\sqrt{\pi \kappa_r t}} \tag{3.24}$$

3.1.4 Dimensionless equations

We first rewrite the different temperatures such that $T = T_0 + (T_i - T_0)\theta$ where $\theta(r,z,t)$ is the equivalent dimensionless temperature. In term of θ, the integral balance approximation (3.13) rewrites

$$\theta(z) = \begin{cases} \Theta_b - (\Theta_b - \Theta_s)\,(1 - \frac{z}{\delta})^2 & 0 \le z \le \delta \\ \Theta_b & \delta \le z \le h - \delta \\ \Theta_b - (\Theta_b - \Theta_s)\,(1 - \frac{h-z}{\delta})^2 & h - \delta \le z \le h \end{cases} \tag{3.25}$$

where $\Theta_b = \frac{T_b - T_0}{T_i - T_0}$ and $\Theta_s = \frac{T_s - T_0}{T_i - T_0}$. Equations (3.18) and (3.7) are nondimensionalized using the same horizontal scale Λ, vertical height scale H and time scale τ used is section 2.2.2 as well as a horizontal velocity scale

$U = \Lambda/\tau = (\rho_m g H^3) / (12\eta_h \Lambda)$ to give

$$\frac{\partial h}{\partial t} = \frac{12}{r}\frac{\partial}{\partial r}\left(r\left(\frac{\partial h}{\partial r} + \frac{\partial}{\partial r}\left(\nabla^4 h\right)\right) I_1(h)\right) + w_i \tag{3.26}$$

$$\begin{aligned}\frac{\partial}{\partial t}\left(\delta(\bar{\theta} - \Theta_b)\right) &= -\frac{1}{r}\frac{\partial}{\partial r}\left(r\delta(\overline{u\theta} - \bar{u}\Theta_b)\right) - \delta\left(\frac{\partial \Theta_b}{\partial t} + \overline{u}\frac{\partial \Theta_b}{\partial r}\right) \\ &- 2Pe^{-1}St_m\frac{(\Theta_b - \Theta_s)}{\delta} + \frac{w_i}{2}(1 - \Theta_b)\end{aligned} \tag{3.27}$$

$$u(r, z, t) = 12\left(\frac{\partial h}{\partial r} + \frac{\partial}{\partial r}\left(\nabla^4 h\right)\right) I_0(z) \tag{3.28}$$

$$w_i = \frac{32}{\gamma^2}\left(\frac{1}{4} - \frac{r^2}{\gamma^2}\right)\left(1 - \frac{h_0}{\sigma}\right) \quad \text{if } r < \gamma/2 \tag{3.29}$$

$$\tag{3.30}$$

with

$$I_0(z) = \int_0^z \frac{1}{\eta(\theta, \nu)}\left(y - \frac{h}{2}\right) dy \tag{3.31}$$

$$I_1(z) = \int_0^z \frac{1}{\eta(\theta, \nu)}\left(y - \frac{h}{2}\right) y dy \tag{3.32}$$

where $\eta(\theta, \nu)$ is the dimensionless rheology η/η_h which depends on the dimensionless temperature θ and the dimensionless number ν. In addition, the thermal boundary conditions (3.23) and (3.24) resume to

$$2\frac{\Theta_b - \Theta_s}{\delta} = \Omega Pe^{1/2}\frac{\Theta_s}{\sqrt{\pi t}}. \tag{3.33}$$

γ, σ, Pe, St_m, ν and Ω are the six dimensionless numbers that control the dynamics of the flow

$$\gamma = \frac{a}{\Lambda} \tag{3.34}$$

$$\sigma = \frac{\Delta P}{\rho_m g h_0} \tag{3.35}$$

$$Pe = \frac{H^2}{\kappa_m \tau} \tag{3.36}$$

$$St_m = \frac{C_{p,m}\left(T_L - T_S\right)}{C_{p,m}\left(T_L - T_S\right) + L} \tag{3.37}$$

$$\nu = \frac{\eta_h}{\eta_c} \tag{3.38}$$

$$\Omega = \frac{k_r}{k_m}\left(\frac{\kappa_m}{\kappa_r}\right)^{1/2} \tag{3.39}$$

γ is the dimensionless radius of the conduit and σ is the normalized pressure head which have been discussed in section 2.2. Pe is the Peclet number, it compares the vertical diffusion of heat to the horizontal advection in the intrusion interior. St_m is a modified Stephan number, it is the ratio of sensible heat between solidus and liquidus to the total energy of the fluid at liquidus temperature and tends to one when the crystallization is neglected. ν is the maximum viscosity contrast, i.e. the ratio between the hottest and coldest viscosity. Ω is the ratio between heat conduction at the contact with the encasing rocks and heat diffusion within the fluid.

3.1.5 Further simplifications

Heat balance equation

The heat balance equations (3.27) can reduce to

$$\frac{\partial}{\partial t}\left(\delta(\bar{\theta}-1)\right)+\frac{1}{r}\frac{\partial}{\partial r}\left(r\delta(\overline{u\theta}-\bar{u})\right) \quad = \quad -2Pe^{-1}St_m\frac{(\Theta_b-\Theta_s)}{\delta} \tag{3.40}$$

Indeed, if the thermal boundary layers exist, $\Theta_b = 1$, δ is the variable and the heat balance equation (3.27) reduces to the equation (3.40). In contrast, if the thermal boundary layers merge, $\delta = h/2$ and the variable is Θ_b. In this case, the heat balance equations (3.27) reduces to:

$$\frac{\partial h\bar{\theta}}{\partial t}+\frac{1}{r}\frac{\partial}{\partial r}\left(rh\overline{u\theta}\right)-\Theta_b\left(\frac{\partial h}{\partial t}+\frac{1}{r}\frac{\partial}{\partial r}\left(rh\bar{u}\right)\right) \quad = \quad -8St_mPe^{-1}\frac{(\Theta_b-\Theta_s)}{h}+w_i(1-\Theta_b)$$

which we can rewrite using (3.26) as

$$\frac{\partial h\bar{\theta}}{\partial t}+\frac{1}{r}\frac{\partial}{\partial r}\left(rh\overline{u\theta}\right)=w_i-8St_mPe^{-1}\frac{(\Theta_b-\Theta_s)}{h}$$

which also corresponds to (3.40) in the case where $\delta = h/2$.

Following *Balmforth and Craster* (2000), we rewrite (3.40) using a new variable $\xi = \delta(1-\bar{\theta})$

$$\frac{\partial \xi}{\partial t}+\frac{1}{r}\frac{\partial}{\partial r}\left(r\bar{u}\xi\right)-\frac{1}{r}\frac{\partial}{\partial r}\left(r\delta(\overline{u\theta}-\bar{u}\bar{\theta})\right)=2Pe^{-1}St_m\frac{(\Theta_b-\Theta_s)}{\delta} \tag{3.41}$$

The second term of the equation contains advection by the vertically integrated radial velocity while the third term contains a correction accounting for the vertical structure of the temperature field. The term on the right is the loss of heat by conduction in the surrounding medium.

Average quantities

The average velocity over a thermal boundary layer $\overline{u}$ reads

$$\overline{u} = \frac{1}{\delta}\int_0^\delta u dz = u(r,\delta,t) - \frac{1}{\delta}\int_0^\delta \frac{\partial u}{\partial z} z dz \tag{3.42}$$

$$= \frac{12}{\delta}\frac{\partial P}{\partial r}\left(\delta I_0(\delta) - I_1(\delta)\right) \tag{3.43}$$

where $P(r,z,t) = h + \nabla^4 h$ is the dimensionless pressure and we have used (3.28). The average advection $\overline{u\theta}$ over a thermal boundary layer reads

$$\overline{u\theta} = \frac{1}{\delta}\int_0^\delta u\theta dz = \frac{1}{\delta}\left([uG(z)]_0^\delta - \int_0^\delta G(z)\frac{\partial u}{\partial z} dz\right)$$

$$= \frac{12}{\delta}\frac{\partial P}{\partial r}\left(G(\delta)I_0(\delta) - I_2(\delta)\right) \tag{3.44}$$

where

$$G(z) = \Theta_b z - \frac{(\Theta_b - \Theta_s)}{3}\delta\left(1 - \frac{z}{\delta}\right)^3 \tag{3.45}$$

denotes a primitive of θ when $z < \delta$ and

$$I_2(z) = \int_0^y \frac{1}{\eta(\theta,\nu)} G(y)\left(y - \frac{h}{2}\right) dy. \tag{3.46}$$

Therefore, we have

$$\overline{u\theta} - \overline{u}\,\overline{\theta} = \frac{12}{\delta}\frac{\partial P}{\partial r}\left(I_0(\delta)\left(G(\delta) - \delta\overline{\theta}\right) + \overline{\theta} I_1(\delta) - I_2(\delta)\right) \tag{3.47}$$

where the average temperature over a thermal boundary layer reads

$$\overline{\theta} = \frac{2}{3}\left(\Theta_b + \Theta_s\right) \tag{3.48}$$

Main variables

The variable ξ is the sufficient variable to solve for in the heat transport equation (3.41). Indeed,

$$\xi = \frac{\delta}{3}\left(-2\Theta_b - \Theta_s + 3\right) \tag{3.49}$$

where we have used (3.48). In addition, from (3.33), we can rewrite

$$\Theta_s = \frac{2\Theta_b}{\beta\delta + 2}, \tag{3.50}$$

$$\delta = \frac{1}{\Theta_s \beta}\left(2\Theta_b - 2\Theta_s\right), \tag{3.51}$$

$$\Theta_b = \frac{\Theta_s}{2}\left(\beta\delta + 2\right) \tag{3.52}$$

where $\beta = \Omega Pe^{1/2}/\sqrt{\pi t}$ for clarity.

When the thermal boundary layer just merged, then $\Theta_b = 1$, $\delta = h/2$ and injecting (3.50) into (3.49) gives

$$\xi_t(t) = \frac{\beta(t)h^2(r,t)}{6\beta(t)h(r,t) + 24} \tag{3.53}$$

Therefore, when $\xi < \xi_t$, the thermal boundary layer are not merged, $\Theta_b = 1$ and injecting (3.51) into (3.49) and solving for Θ_s gives

$$\Theta_s = \frac{3\beta}{4}\xi - \frac{\sqrt{3}}{4}\sqrt{\beta\xi\left(3\beta\xi + 8\right)} + 1. \tag{3.54}$$

In contrast, when $\xi > \xi_t$, the thermal boundary layer are merged, $\delta = h/2$ and injecting (3.52) into (3.49) and solving for Θ_s gives

$$\Theta_s = \frac{-12\xi + 6h}{\left(\beta h + 6\right)h}. \tag{3.55}$$

3.1.6 Summary of the equations

The equation governing the cooling of an elastic-plated gravity current with rheology $\eta(\theta, \nu)$ are summarized as follow

$$\frac{\partial h}{\partial t} - \frac{12}{r}\frac{\partial}{\partial r}\left(rI_1(h)\left(\frac{\partial}{\partial r}\left(h + \nabla^4 h\right)\right)\right) = w_i \tag{3.56}$$

$$\frac{\partial \xi}{\partial t} + \frac{1}{r}\frac{\partial}{\partial r}\left(r\left(\bar{u}\xi - \Sigma\right)\right) = 2Pe^{-1}St_m\frac{\left(\Theta_b - \Theta_s\right)}{\delta} \tag{3.57}$$

where

$$\Theta_s(r,t) = \begin{cases} \frac{3\beta}{4}\xi - \frac{\sqrt{3}}{4}\sqrt{\beta\xi\left(3\beta\xi + 8\right)} + 1 & \text{if} \quad \xi \leq \xi_t \\ \frac{-12\xi + 6h(r,t)}{(\beta h(r,t) + 6)h(r,t)} & \text{if} \quad \xi > \xi_t \end{cases} \tag{3.58}$$

$$\Theta_b(r) = \begin{cases} 1 & \text{if} \quad \xi \leq \xi_t \\ \frac{\Theta_s}{4}\left(\beta(t)h(r,t) + 4\right) & \text{if} \quad \xi > \xi_t \end{cases} \tag{3.59}$$

$$\delta(r) = \begin{cases} \frac{1}{\Theta_s\beta(t)}\left(-2\Theta_s + 2\right) & \text{if} \quad \xi \leq \xi_t \\ h(r,t)/2 & \text{if} \quad \xi > \xi_t \end{cases} \tag{3.60}$$

with

$$\xi_t(t) = \frac{\beta(t)h^2(r,t)}{6\beta(t)h(r,t)+24} \tag{3.61}$$

$$\beta(t) = \Omega Pe^{1/2}\frac{1}{\sqrt{\pi t}} \tag{3.62}$$

$$\overline{u} = \frac{12}{\delta}\left(\frac{\partial}{\partial r}\left(h+\nabla^4 h\right)\right)\left(\delta I_0(\delta) - I_1(\delta)\right) \tag{3.63}$$

$$\Sigma = 12\left(\frac{\partial}{\partial r}\left(h+\nabla^4 h\right)\right)\left(I_0(\delta)\left(G(\delta)-\delta\overline{\theta}\right)+\overline{\theta}I_1(\delta)-I_2(\delta)\right) \tag{3.64}$$

$$\overline{\theta} = \frac{2}{3}\left(\Theta_b+\Theta_s\right) \tag{3.65}$$

$$G(z) = \Theta_b z - \frac{(\Theta_b-\Theta_s)}{3}\delta\left(1-\frac{z}{\delta}\right)^3 \tag{3.66}$$

$$w_i = \frac{32}{\gamma^2}\left(\frac{1}{4}-\frac{r^2}{\gamma^2}\right)\left(1-\frac{h_0}{\sigma}\right) \tag{3.67}$$

and

$$I_0(z) = \int_0^z \frac{1}{\eta(\theta,\nu)}\left(y-\frac{h}{2}\right)dy \tag{3.68}$$

$$I_1(z) = \int_0^z \frac{1}{\eta(\theta,\nu)}\left(y-\frac{h}{2}\right)ydy \tag{3.69}$$

$$I_2(z) = \int_0^y \frac{1}{\eta(\theta,\nu)}\left(y-\frac{h}{2}\right)G(y)dy. \tag{3.70}$$

$$\tag{3.71}$$

3.2 Numerical approach

3.2.1 General procedure

The coupled nonlinear partial differential equations (3.56) and (3.57) are solved on a grid of size M defined by the relation $r_i = (i-0.5)\Delta r$ for $i = 1,..,M$. The grid is shifted at the center to avoid problem arising from the axisymmetrical geometry. We index the grid point by the indice i and denote the solution on this grid h_i and ξ_i and the secondary variables $\Theta_{b,i}$, $\Theta_{s,i}$ and δ_i. Both equations can be expressed on the convenient form

$$\frac{\partial u}{\partial t} - f = 0 \tag{3.72}$$

where u is the function we want to integrate and f a non-linear function that depends on u. We solve these equations by first discretizing all the spatial

derivatives using Finite Difference. The accuracy of the scheme is determined by the higher order derivatives since their numerical approximation requires the largest number of sample points. We then get two systems of M ordinary differential equations with the form

$$\frac{\partial u_i}{\partial t} - f_i = 0 \qquad i = 1, ..., M \tag{3.73}$$

The time derivatives are first order and, since explicit schemes tend to be very sensitive and unstable, we use a fully implicit backward Euler scheme to get

$$\frac{u_i^{n+1} - u_i^n}{\Delta t} - f_i(u_i^{n+1}) = 0 \qquad i = 1, ..., M \tag{3.74}$$

Since $f_i(u_i^{n+1})$ is not a linear function, the system above cannot be re-arranged to solve u_i^{n+1} in term of u_i^n and an iterative method has to be employed instead. Fixed point iteration method have shown poor results in converging toward the solution and we finally apply second order Newton's method to obtain the solution at each time step. In particular, we first linearize u^{n+1} around a guess of the solution by assuming $u^{n+1} = u^* + \delta u^n$, where u^* is a guess and δu^n is the error and we drop the i for clarity. Then, we expressed the non-linear part using a Taylor's expansion

$$f^{n+1} = f(u^{n+1}) = f(u^* + \delta u^n) = f(u^*) + J_f^h(u^*)\delta u^n$$

where $J_f^u(u^*)$ is the jacobian matrix for the function f evaluated in h^*. Injecting the expansion into (3.74) finally gives a system of M linear equations for the correction term δ_h^n which can be expressed as

$$(I - \Delta t J_f^u(u^*))\delta u^n = u^n - u^* + \Delta t f(u^*) \tag{3.75}$$

where I is the identity matrix. Therefore, each iteration solves for δu^n and we use $u_n + \delta u^n$ as a new guess u^* in each iteration. This is repeated until δu^n becomes sufficiently small. Finally, since the equations are coupled, we use a fixed-point iteration method to converge toward the solution (h, ξ) at each time step. Therefore, the algorithm is the following at each time step

- Start with a guess for the values of all variables.
- Solve the thickness equation (3.56) for h^{n+1} using Newton-Rhapsod method.
- Solve the heat equation (3.57) for ξ^{n+1} using h^{n+1} as a new guess for h^* and Newton-Rhapsod method.
- Repeat step one until further iterations cease to produce any significant changes in the values of both h^{n+1} and ξ^{n+1}.

The computational scheme is summarized in the following.

3.2.2 Thickness equation

The thickness equation (3.56) is written as

$$\frac{\partial h}{\partial t} - f(h,\xi) = 0 \tag{3.76}$$

with

$$f = \frac{1}{r}\frac{\partial}{\partial r}\left(r\phi\left(\frac{\partial}{\partial r}(h+P)\right)\right) + w_i \tag{3.77}$$

$$\phi = 12 I_1(h) \tag{3.78}$$

and where P is the dimensionless bending pressure $P = \nabla^4 h$.

Spatial discretization of f

The spatial discretization is obtained using a central difference scheme over a sub-grid shifted by $0.5\Delta r$ from the main grid. Therefore, we have

$$\begin{aligned} f_i &= \frac{1}{r_i \Delta_r}\left(r_{i+1/2}\phi_{i+1/2}\left(\frac{\partial h}{\partial r}+\frac{\partial P}{\partial r}\right)\Big|_{i+1/2} - r_{i-1/2}\phi_{i-1/2}\left(\frac{\partial h}{\partial r}+\frac{\partial P}{\partial r}\right)\Big|_{i-1/2}\right) \\ &= A_i\phi_{i+1/2}(h_{i+1}-h_i) - B_i\phi_{i-1/2}(h_i - h_{i-1}) \\ &+ A_i\phi_{i+1/2}(P_{i+1}-P_i) - B_i\phi_{i-1/2}(P_i - P_{i-1}) \\ &+ w_i \end{aligned} \tag{3.79}$$

where $A_i = r_{i+1/2}/(r_i\Delta_r^2)$ and $B_i = r_{i-1/2}/(r_i\Delta_r^2)$. The bending pressure term P is very stiff and needs a careful treatment. In particular, the fourth order derivative requires a fourth order central difference scheme and therefore, P_i is expressed over a seven point stencil on the main grid such that

$$P_i = \alpha_i h_{i-3} + \beta_i h_{i-2} + \gamma_i h_{i-1} + \lambda_i h_i + \kappa_i h_{i+1} + \delta_i h_{i+2} + \varepsilon_i h_{i+3} \tag{3.80}$$

with

$$\begin{aligned} \alpha_i &= \frac{1}{24\Delta r^4}(-4+3p_3\Delta_r) \\ \beta_i &= \frac{1}{24\Delta r^4}\left(48-24p_3\Delta_r - 2p_2\Delta_r^2 + 2p_1\Delta_r^3\right) \\ \gamma_i &= \frac{1}{24\Delta r^4}\left(-156+39p_3\Delta_r + 32p_2\Delta_r^2 - 16p_1\Delta_r^3\right) \\ \lambda_i &= \frac{1}{24\Delta r^4}\left(224-60p_2\Delta r^2\right) \\ \kappa_i &= \frac{1}{24\Delta r^4}\left(-156-39p_3\Delta_r + 32p_2\Delta_r^2 + 16p_1\Delta_r^3\right) \\ \delta_i &= \frac{1}{24\Delta r^4}\left(48+24p_3\Delta_r - 2p_2\Delta_r^2 - 2p_1\Delta_r^3\right) \\ \varepsilon_i &= \frac{1}{24\Delta r^4}(-4-3p_3\Delta_r) \end{aligned}$$

and where $p_1 = 1/r_i^3$, $p_2 = 1/r_i^2$ and $p_3 = 2/r_i$. Finally, the term $\phi_{i-1/2}$ and $\phi_{i-1/2}$, which depend on the variable Θ_b, δ as well as different power of h, are evaluated in $i - 1/2$ and $i + 1/2$ respectively. Different choices for the value of the variable at the mid-cell grid point do not show any significant difference and a simple average is taken such that the variable $u_{i+1/2}$ is taken as $0.5(u_i + u_{i+1})$.

Expression of the jacobian J_f^h

The discretized function f_i can be break down in three part, the gravitational part f_i^g which is expressed in term of the value of h on three grid points $\{i-1, i, i+1\}$, the bending part f_i^b which is expressed in term of the value of h on nine grid points $\{i-4, i-3, ..., i+3, i+4\}$ and the injection term which depends only on the grid point i such that

$$f_i = f_i^g + f_i^b + w_i \tag{3.81}$$

Therefore, the jacobian is nona-diagonal and its coefficient J_{il} are

$$J_{il} = \begin{cases} \frac{\partial f_i^b}{\partial h_l} & l = \{i-4, i-3, i-2, i+2, i+3, i+4\} \\ \frac{\partial f_i^g}{\partial h_l} + \frac{\partial f_i^b}{\partial h_l} & l = \{i-1, i, i+1\} \\ 0 & \text{otherwise} \end{cases} \tag{3.82}$$

The different terms can be easily derived from (3.79) and (3.80) with just slight adjustment coming from the boundary conditions.

Boundary condition

We begin with $h_i = h_f$ for $i = 1, .., M$. Since the flow is symmetric in $r = 0$, we require that

$$\left.\frac{\partial h}{\partial r}\right|_{r=0} = \left.\frac{\partial P}{\partial r}\right|_{r=0} = 0 \tag{3.83}$$

and therefore for $i = 1$, we have

$$\begin{aligned} f_i &= A_1 \phi_{i+1/2} \left(h_{i+1} - h_i\right) \\ &+ A_i \phi_{i+1/2} \left(P_{i+1} - P_i\right) \\ &+ w_i \end{aligned} \tag{3.84}$$

The expression of the bending pressure, evaluated over a 7 point stencils, is problematic close to the boundary and reflection formulae will be used in order to accommodate the boundary conditions *Patankar* (1980). In particular, we have $h_0 = h_1$, $h_{-1} = h_2$ and $h_{-2} = h_3$. Similarly, boundary condition at the

end of the mesh is accounted by using a grid much larger than the flow itself and requiring

$$\left.\frac{\partial h}{\partial r}\right|_{r=r_M} = \left.\frac{\partial P}{\partial r}\right|_{r=r_M} = 0 \tag{3.85}$$

which gives for $i = M$

$$\begin{aligned} f_i &= B_i\phi_{i-1/2}\left(h_i - h_{i-1}\right) \\ &+ B_i\phi_{i-1/2}\left(P_i - P_{i-1}\right) \\ &+ w_i \end{aligned} \tag{3.86}$$

with $h_{i>=M} = h_f$.

Newton-Rhapsod method

The Newton-Rhapsod method reads

$$(I - \Delta t J_f^h(h_k^*))\delta h_k^n = h^n - h_k^* + \Delta t f(h_k^*) \tag{3.87}$$

where the k refers to the k iterations, I is a $M \times M$ diagonal matrix and $J_f^h(h^*)$ is a $M \times M$ nona-diagonal matrix. This system of linear equations can be solved using a nona-diagonal algorithm. At the first iteration, we use $h_1^* = h^n$ as a first guess and then we iterate using $h_k^* = h^n + \delta h_{k-1}^n$ as a new guess for each iterations until δh_k^n becomes sufficiently small. In particular, we require that

$$\delta h_k^n / h_k^* < \varepsilon \tag{3.88}$$

with $\varepsilon = 10^{-4}$.

3.2.3 Heat equation

The heat equation (3.57) is written as

$$\frac{\partial \xi}{\partial t} - g(h, \xi) = 0 \tag{3.89}$$

with

$$g = \frac{1}{r}\frac{\partial}{\partial r}\left(r\Gamma\xi\right) + \frac{1}{r}\frac{\partial}{\partial r}\left(r\Sigma\right) + 2Pe^{-1}St_m\frac{(\Theta_b - \Theta_s)}{\delta} \tag{3.90}$$

$$\Gamma = -\overline{u} \tag{3.91}$$

Spatial discretization of g

As for the thickness equation, the spatial discretization is obtained using a central difference scheme over a sub-grid shifted by $0.5\Delta r$ from the main grid. Therefore, we have

$$\begin{aligned} g_i &= \left(C_i\Gamma_{i+1/2}\xi_{i+1/2} - D_i\Gamma_{i-1/2}\xi_{i-1/2}\right) && (3.92)\\ &+ \left(C_i\Sigma_{i+1/2} - D_i\Sigma_{i-1/2}\right) && (3.93)\\ &+ 2Pe^{-1}St_m\frac{\Theta_{b,i}-\Theta_{s,i}}{\delta_i} && (3.94)\end{aligned}$$

with $C_i = r_{i+1/2}/(r_i\Delta r)$ and $D_i = r_{i-1/2}/(r_i\Delta r)$. We use the average between the grid point i and $i-1$ (resp. $i+1$) to evaluate the quantity in Γ and Σ at $i-1/2$ (resp. $i+1/2$). In addition, we use a classical upwind scheme to handle ξ at the mid grid point which requires

$$\begin{aligned} \xi_{i+1/2} &= \xi_i && (3.95)\\ \xi_{i-1/2} &= \xi_{i-1} && (3.96)\end{aligned}$$

Expression of the Jacobian J_g^ξ

The expression of the Jacobian is much straightforward in that case and its coefficient J_{il} are

$$J_{il} = \begin{cases} -D_i\Gamma_{i-1/2} & l = i-1 \\ C_i\Gamma_{i+1/2} & l = i \\ 0 & \text{otherwise} \end{cases} \qquad (3.97)$$

with only slight adjustment coming from the boundary conditions.

Boundary conditions

We consider $\Theta_b = 1$ and $\delta = 10^{-4}$ in the film at $t = 0$. In this way, we ensure that the average temperature across the film at $t = 0$ is close to 1. By construction, $D_1 = 0$ and therefore, for $i = 1$ we have

$$g_i = C_i\Gamma_{i+1/2}\xi_i + C_i\Sigma_{i+1/2} + 2Pe^{-1}St_m\frac{\Theta_{b,i}-\Theta_{s,i}}{\delta_i} \qquad (3.98)$$

For $i = M$, we consider that $\Gamma_{i+1/2} = \Gamma_i$ and $\Sigma_{i=1/2} = \Sigma_i$. However, the choice for the boundary condition at the border of the grid $i = M$ is not important as we solve the problem over a grid much larger than the flow itself.

Newton-Rhapsod method

The Newton-Rhapsod method reads

$$(I - \Delta t J_g^{\xi}(\xi_k^*))\delta\xi_k^n = \xi^n - \xi_k^* + \Delta t f(\xi_k^*) \tag{3.99}$$

where the k refers to the k iterations, I is a $M \times M$ diagonal matrix and $J_f^h(\xi^*)$ is a $M \times M$ tri-diagonal matrix. This system of linear equations can be solved using a tri-diagonal algorithm. As for the thickness equation, at the first iteration, we use $\xi_1^* = \xi^n$ as a first guess and then we iterate using $\xi_k^* = \xi^n + \delta\xi_{k-1}^n$ as a new guess for each iterations until $\delta\xi_k^n$ becomes sufficiently small. In particular, we require that

$$\delta\xi_k^n / \xi_k^* < \varepsilon \tag{3.100}$$

with $\varepsilon = 10^{-4}$. In addition, at each iteration the quantity $\Theta_{s,k}^*$, $\Theta_{b,k}^*$ and δ_k^*, that are needed to evaluate Γ and Σ, are derived from the value of ξ_k^* using (3.58), (3.59) and (3.60) respectively.

Chapter 4

First order modelling - Isothermal rocks

Chapter 5

Second order modelling

Contents

The previous chapter was first step toward the understanding how the cooling of the laccolith interact with its dynamics.

A simple model have been developed in chapter 4.

5.1 Influence of the flow rheology

5.2 Heating of the surrounding layer

5.3 Crystallization

5.4 Applications

Part III

Theoretical model for isothermal crater-centered intrusion

Chapter 6

Second order modelling

Contents

The previous chapter was first step toward the understanding how the cooling of the laccolith interact with its dynamics.

A simple model have been developed in chapter 4.

6.1 Influence of the flow rheology

6.2 Heating of the surrounding layer

6.3 Crystallization

6.4 Applications

Chapter 7

Floor-fractured craters

Chapter 8

Gravitationnal signature of lunar floor-fractured craters

Bibliography

Balmforth, N. J., and R. V. Craster (2000), Dynamics of cooling domes of viscoplastic fluid, *Journal of Fluid Mechanics*. (Cited on pages 22 and 26.)

Bertozzi, A. L. (1998), The mathematics of moving contact lines in thin liquid films, *Notices AMS*. (Cited on page 12.)

Bunger, A. P., and A. R. Cruden (2011), Modeling the growth of laccoliths and large mafic sills: Role of magma body forces, *Journal of Geophysical Research*, *116*(B2), B02,203. (Cited on pages 7 and 12.)

Carslaw, H. S., and J. C. Jaeger (1959), Heat in solids. (Cited on page 24.)

Flitton, J. C., and J. R. King (2004), Moving-boundary and fixed-domain problems for a sixth-order thin-film equation, *European Journal of Applied Mathematics*, *15*(06), 713–754. (Cited on page 12.)

Goodman, T. R. (1958), *The heat-balance integral and its application to problems involving a change of phase*, Trans. ASME. (Cited on page 22.)

Hewitt, I. J., N. J. Balmforth, and J. R. De Bruyn (2014), Elastic-plated gravity currents, pp. 1–29. (Cited on pages 7 and 12.)

Hort, M. (1997), Cooling and crystallization in sheet-like magma bodies revisited, *Journal of Volcanology and Geothermal Research*, *76*(3-4), 297–317. (Cited on page 22.)

Huppert, H. E. (1982), The propagation of two-dimensional and axisymmetric viscous gravity currents over a rigid horizontal surface, *Journal of Fluid Mechanics*, *121*(-1), 43–58. (Cited on page 14.)

Johnson, A. M., and D. D. Pollard (1973), Mechanics of growth of some laccolithic intrusions in the Henry mountains, Utah, I: field observations, Gilbert's model, physical properties and flow of the magma, *Tectonophysics*. (Cited on page 7.)

Lister, J. R., G. G. Peng, and J. A. Neufeld (2013), Viscous Control of Peeling an Elastic Sheet by Bending and Pulling, *Physical Review Letters*, *111*(15), 154,501. (Cited on pages 8, 12, 13 and 14.)

McKenzie, D. (1984), The Generation and Compaction of Partially Molten Rock, *Journal of Petrology*, *25*(3), 713–765. (Cited on pages 5 and 6.)

McKenzie, D. (1985), The extraction of magma from the crust and mantle, *Earth and Planetary Science Letters*, *74*(1), 81–91. (Cited on pages 5 and 6.)

Michaut, C. (2011), Dynamics of magmatic intrusions in the upper crust: Theory and applications to laccoliths on Earth and the Moon, *Journal of Geophysical Research*, *116*(B5), B05,205. (Cited on pages 7, 11, 12, 13, 14, 15 and 19.)

Michaut, C., and D. Bercovici (2009), A model for the spreading and compaction of two-phase viscous gravity currents, *Journal of Fluid Mechanics*, *630*, 299–329. (Cited on page 11.)

Michaut, C., and C. Jaupart (2006), Ultra-rapid formation of large volumes of evolved magma, *Earth and Planetary Science Letters*, *250*(1-2), 38–52. (Cited on page 22.)

Michaut, C., D. Baratoux, and C. Thorey (2013), Magmatic intrusions and deglaciation at mid-latitude in the northern plains of Mars, *Icarus*, *225*(1), 602–613. (Cited on page 8.)

Miller, R. B., and S. R. Paterson (1999), In defense of magmatic diapirs, *Journal of Structural Geology*, *21*(8-9), 1161–1173. (Not cited.)

Patankar, S. (1980), Numerical heat transfer and fluid flow. (Cited on page 32.)

Petford, N., A. R. Cruden, K. J. W. McCaffrey, and J. L. Vigneresse (2000), Granite magma formation, transport and emplacement in the Earth's crust, *Nature*, *408*(6813), 669–673. (Cited on page 5.)

Pollard, D. D., and A. M. Johnson (1973), Mechanics of growth of some laccolithic intrusions in the Henry Mountains, Utah, II: bending and failure of overburden layers and sill formation, *Tectonophysics*, *18*(3-4), 311–354. (Cited on page 7.)

Snoeijer, J. H., and B. Andreotti (2013), Moving Contact Lines: Scales, Regimes, and Dynamical Transitions, *Annual Review of Fluid Mechanics*, *45*(1), 269–292. (Cited on page 12.)

Turcotte, D. L., and G. Schubert (1982), Geodynamics: Applications of continuum physics to geological problems, John Wiley, New York. (Cited on page 9.)